

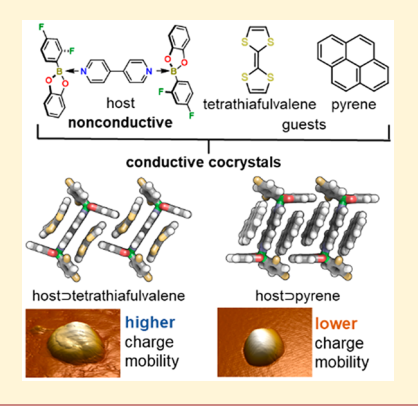
Semiconductor Cocrystals Based on Boron: Generated Electrical Response with π -Rich Aromatic Molecules

Published as part of a Crystal Growth and Design virtual special issue Remembering the Contributions and Life of Prof. Joel Bernstein

Kamal K. Ray,^{†,#} Gonzalo Campillo-Alvarado,^{†,#} Hugo Morales-Rojas,[‡] Herbert Höpfl,*^{,‡} Leonard R. MacGillivray, ** † o and Alexei V. Tivanski ** † o

Supporting Information

ABSTRACT: Cocrystallization of a nonconductive, boron-based host with aromatic guests generates conductive cocrystals. Carrier mobilities of the cocrystals with either pyrene or tetrathiafulvalene were measured using conducting probe atomic force microscopy. The incorporation of the π -electron-rich aromatic guests results in electrically conductive cocrystals. The cocrystal with tetrathiafulvalene as a guest shows an approximately seven times higher charge carrier mobility than the cocrystal with pyrene.



In the rapidly evolving field of molecular electronics, π conjugated organic semiconductors (OSCs) are highly promising for applications as field effect transistors, light emitting diodes, and in photovoltaics. The versatility of OSCs relies on the possibility of tailoring electrical conductivity by both selecting molecules with prerequisite electronic properties and applying strategies to influence molecular packing.

Crystal engineering of OSCs³⁻⁵ aims to promote π -stacking of organics through either covalent or noncovalent methods. While covalent methods (e.g., bulky substituents, 6,7 foldamer structures, 8,9 heteroatoms, 10 and extended aromatics 11) have arguably received the most attention, the noncovalent approach (e.g., cocrystal formation 12-14), which involves the combination and assembly of multiple organic building blocks, remains promising owing to its modularity and relative ease of synthesis. Generally, a promising and successful approach to OSCs based on noncovalent bonds will involve building blocks that (i) self-assemble to form either face-to-face or face-to-edge π -stacks, (ii) generate persistent extended stacking, and (iii) afford variability of electrical response. A combination of faceto-face and face-to-edge stacking for example facilitates high charge carrier mobilities in solids based on a herringbone structure.⁴ A recent report¹⁴ involving pseudorotaxanes cocrystallized with phenazines highlights the noncovalent approach.

Herein, we describe a solid-state ordering strategy based on cocrystallization of the diboronate adduct **BEA** with π -rich

aromatics (Scheme 1). We show BEA to act as a host by forming cocrystals with either tetrathiafulvalene (TTF) or pyrene (PYR) as guests. BEA self-assembles with each aromatic guest to form persistent one-dimensional (1D) stacks based on a combination of face-to-face $\pi \cdots \pi$ and face-to-edge $C-H\cdots\pi$ contacts. The integration of one additional equivalent of the π -rich aromatics in solids with **BEA** enables the generation of infinite columns with concomitant variability of the electrical conduction properties. Using conducting probe atomic force microscopy (CP-AFM), the cocrystal of BEA with TTF displays an approximately seven times higher charge carrier mobility compared to BEA PYR, while guest-free BEA is an insulator. The difference in the electrical response is confirmed by diffuse-reflectance UV-vis spectroscopy (UVvis DRS), where larger band gaps correspond to smaller charge carrier mobilities. We expect the ability to confer charge mobility to a boron-based, nonconductive solid using the cocrystal strategy will constitute a valuable tool for the construction of next-generation semiconducting materials.

Our design exploits the reversible dative $B \leftarrow N$ bond of boronic esters and pyridines that produce diboronate adducts with two cavities each for guest inclusion (i.e., tweezers). $^{15-17}$

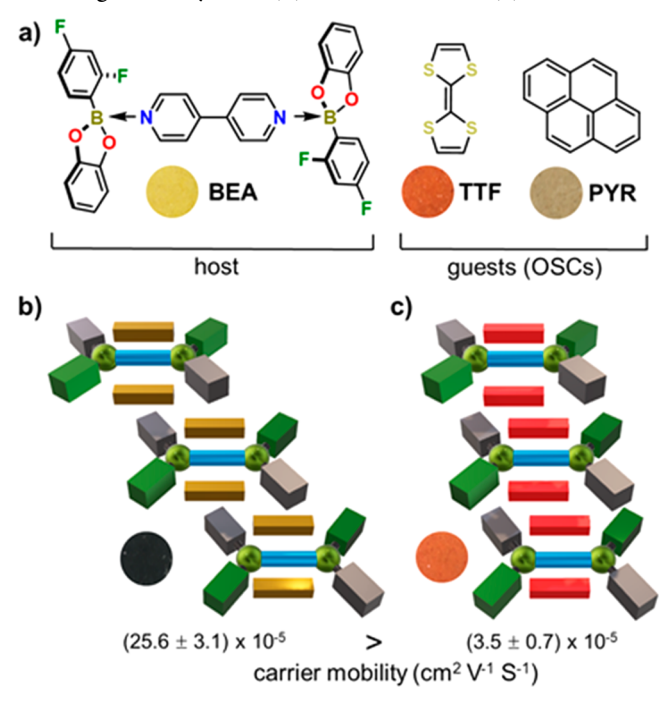
Received: July 18, 2019 Revised: November 11, 2019 Published: November 19, 2019



[†]Department of Chemistry, University of Iowa, Iowa City, Iowa 52242, United States

[‡]Centro de Investigaciones Químicas, Universidad Autónoma del Estado de Morelos, Av. Universidad 1001, 62209, Cuernavaca, México

Scheme 1. (a) Host BEA, Guests TTF and PYR, and π -Stacking of Cocrystals, (b) BEA \supset TTF, and (c) BEA \supset PYR^a



^aCircles indicate the color of the solid.

The 4,4'-bipyridine linkers in **BEA** are electron-deficient upon $B \leftarrow N$ bond formation; thus, we hypothesized the ability of **BEA** to include π -rich guests in combination with a known enhancement of charge mobility conferred by the $B \leftarrow N$ bond could be used to generate organic semiconductor solids. We targeted **TTF** and **PYR** as guests owing to their propensities to form π -stacks that lead to semiconductor behavior (Figure 1a,b). The diboron adduct itself self-assembles in a herringbone arrangement that we also show here is nonconductive (Figure 1c).

Cocrystals of BEA \supset TTF and BEA \supset PYR were synthesized following an adapted procedure (see section S1, Supporting Information). Multicomponent crystallization of boronic ester (be) and 4,4'-bipyridine (bpy) with either TTF or PYR (2:1:3 molar ratio) in warm acetonitrile (3 mL) afforded millimetersized single crystals as prisms after a period of 2 days. The components of BEA \supset TTF crystallize in the triclinic space group $P\overline{1}$. The asymmetric unit comprises a half-molecule of BEA and one and a half molecules of TTF. Two boronic ester molecules interact with bpy via B \leftarrow N bonds (1.652(3) Å) of tetrahedral character (THC) of 78% 12 that compares favorably

with related adducts. ^{17,22,23} The pyridyl rings are approximately perpendicular (87.3°) to the plane of atoms C1, O1, and O2 (Figure 2a). As a consequence of the self-assembly

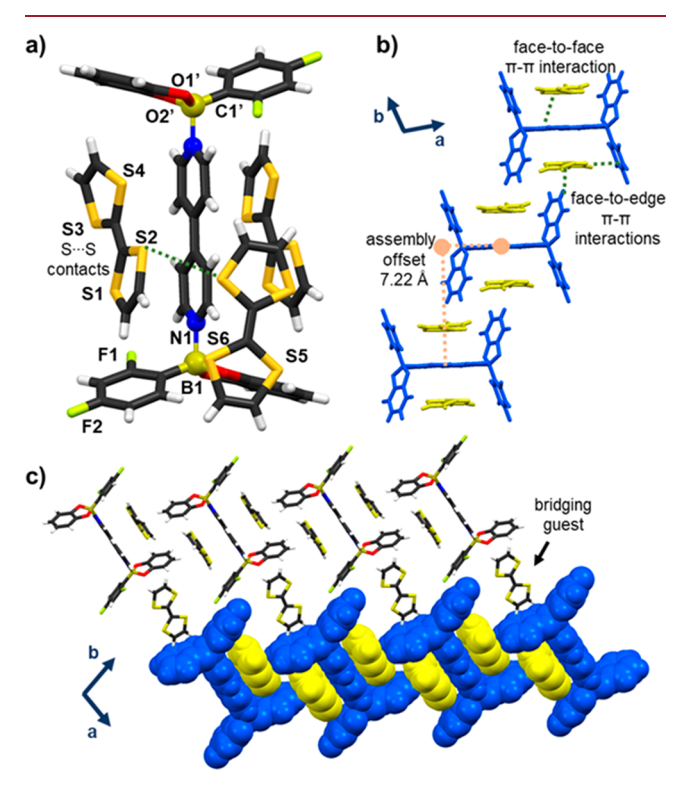


Figure 2. X-ray structure **BEA** \supset **TTF**: (a) stacking of **TTF** with **BEA**, (b) π -stacked column, and (c) view of packing highlighting additional **TTF**.

process, the B \leftarrow N coordination affords a diboronate sandwich adduct with two molecules of TTF interacting with BEA through face-to-face and face-to-edge $\pi\cdots\pi$ forces. The stacking is further propagated with an offset (7.22 Å) as extended columns approximately along the b-axis (Figure 2b). Importantly, the included TTF molecules assume a boat conformation (angle between ring planes = 19.3°) that is indicative of a charge-transfer complex, with TTF and bpy being electron rich and poor, respectively. Additional TTF molecules bridge neighboring π -stacked columns though C-H··· π forces to generate two-dimensional (2D) layers in the ab-plane (Figure 2c). The presence of S···S forces was also observed in the assembly.

For BEA \supset PYR, the components also crystallize in the triclinic space group $P\overline{1}$. Similar to BEA \supset TTF, the asymmetric

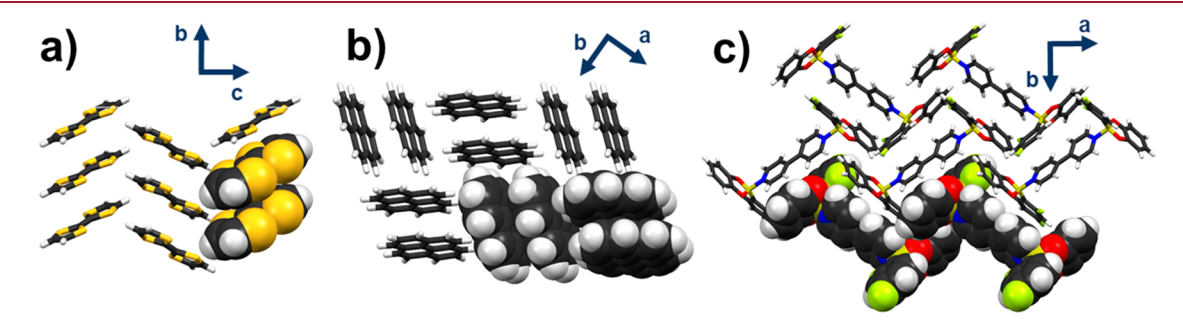


Figure 1. Packings of (a) TTF, (b) PYR, and (c) BEA.

unit contains one-half molecule of BEA and one and a half molecules of PYR (Figure 3). The components form a

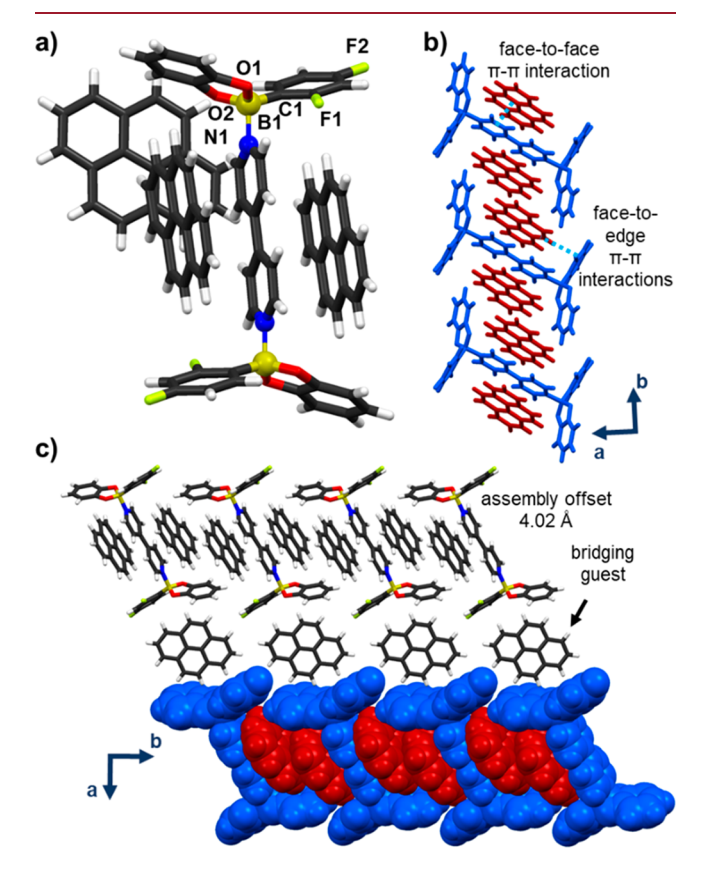


Figure 3. X-ray structure **BEA** \supset **PYR**: (a) stacking of **PYR** with **BEA**, (b) π -stacked column, and (c) extended packing highlighting additional **PYR**.

sandwich complex (B \leftarrow N bond = 1.654(3) Å, THC = 80%, pyridyl-boronic ester orientation 86.8°), in which two **PYR** molecules participate in face-to-face and face-to-edge $\pi \cdots \pi$ forces (Figure 3a). The stacking is less offset (4.02 Å) than for **BEA** \supset **TTF** yielding efficient face-to-face π -stacking along the b-axis (Figure 3b). Importantly, an overall stacking arrangement along the direction of the b-axis is persistent in both cocrystals, with additional **PYR** entities bridging adjacent stacks (Figure 3c, Table S3).

While crystals of guest-free BEA are yellow, the cocrystals BEA⊃PYR and BEA⊃TTF are red and dark blue, respectively. The differences in color are indicative of charge transfer ¹⁴ and variability in band gap energies. Diffuse-reflectance UV—vis spectroscopy (UV—vis DRS) was used to determine the band gap of each solid using a UV—vis NIR Agilent Cary 5000 spectrophotometer. The measurement was carried out on the powder sample at room temperature and under ambient pressure. First, the percentage of reflectance (R, %) versus wavelength (λ , nm) was measured. The R versus λ data were then converted to the fraction of reflectance, F(R), using the Kubelka—Munk function. ^{25,26}

$$F(R) = \frac{(1-R)^2}{2R} \tag{1}$$

The band gap of each solid was calculated using modified Tauc's plot, $^{2.7-29}$ where the direct optical band gap can be determined by first plotting $(F(R)*h\nu)^2$ versus energy = $h\nu$

(Figure 4), then fitting the linear portion of the data within the energy range below the one that corresponds to the maximum

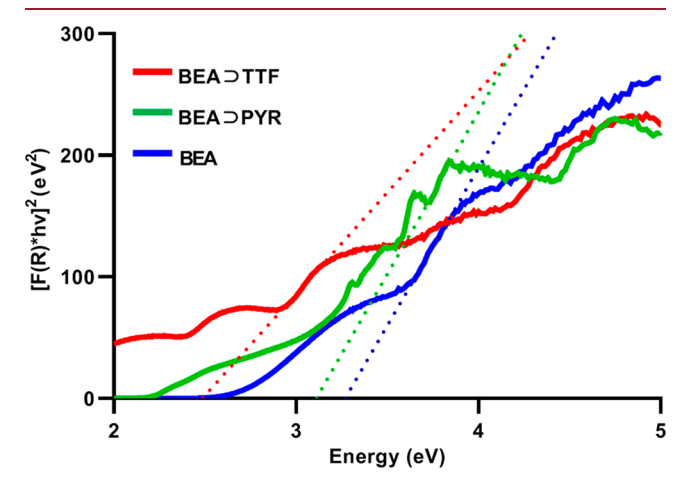


Figure 4. $(F(R)*h\nu)^2$ versus energy = $h\nu$ spectra for BEA⊃PYR, BEA⊃TTF, and BEA. The dotted line represents the fit to straight line for each solid within the linear energy range at and below the energy that corresponds to the maximum reflectance.

reflectance. The fitted energy ranges were 3.90–3.65 eV, 3.15–2.90 eV, and 3.65–3.85 eV for the BEA, BEA \supset TTF, and BEA \supset PYR, respectively. The band gap for each solid was determined by extrapolating each straight line to zero $(F(R)*h\nu)^2$ value, which corresponds to zero absorption. ^{27–29}

The UV—vis DRS of each solid revealed both cocrystals to exhibit lower band gap energies (BEA⊃TTF 2.5 eV, BEA⊃PYR 3.1 eV) compared to BEA (3.3 eV). The lower band gap energies and the face-to-face and face-to-edge π-stacking demonstrated by the X-ray structure data suggest BEA⊃TTF and BEA⊃PYR can display more efficient electrical conduction properties compared to BEA.

Conducting probe AFM (CP-AFM) was used to examine electrical (charge carrier mobility) and mechanical (Young's modulus, YM) properties of individual nanocrystals of BEA, BEA¬TTF, and BEA¬PYR (see sections S4–S6, Supporting Information). CP-AFM provides a unique ability to simultaneously measure the morphology, electrical, and mechanical properties of nanodimensional materials, which is generally not possible with more conventional techniques. Nanodimensional solids are of particular interest owing to a possibility to observe physical—chemical properties that are unique to the length scale. For the CP-AFM measurements, nanosized materials were generated by mortar-and-pestle grinding of the millimeter-sized solids.

AFM height imaging revealed nanocrystals of irregular round morphologies with base sizes of 250–750 nm and heights of 20–100 nm (Figure 5a–c). AFM nanoindentation data and the Johnson–Kendall–Roberts (JKR) contact model were utilized to determine Young's moduli and contact areas between the conductive AFM tip and the nanocrystals (see section S5, Supporting Information).^{33,34} The JKR contact model was selected as there was no hysteresis between the approach and retract data except for the presence of the adhesion force between the AFM tip and nanocrystal. This enabled determination of the current density *J* defined as the measured electrical current divided by the calculated contact area obtained using the JKR contact model (Figure 5d,e). The

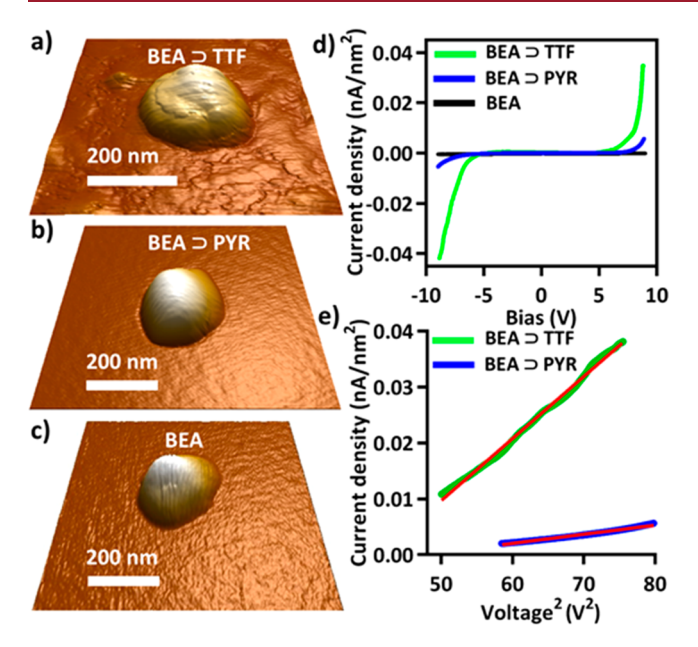


Figure 5. CP-AFM data: (a-c) height images of individual nanocrystals BEA⊃TTF, BEA⊃PYR, and BEA (each crystal height ~55 nm), (d) plots of current density versus surface bias, and (e) plots of current density versus surface bias squared (voltage²) showing a linear response fit to a straight line (red).

higher current density indicates higher electrical conduction through the solid.

Importantly, the adduct BEA showed no detectable electrical conduction (i.e., no measurable current within a detection limit of 10 pA over ±10 V applied biases), which implies insulating behavior. Both BEA¬TTF and BEA¬PYR, however, clearly displayed semiconducting behavior, as evidenced by the absence of electrical current for lower applied biases and a nonlinear increase of the absolute current with increasing absolute surface biases (Figure 5d). Here, the surface bias is external voltage applied to the conductive substrate on which nanocrystals were deposited. BEA¬TTF showed a higher current density compared to BEA¬PYR, thus indicating better electrical conduction and likely a larger charge carrier mobility.

The Mott-Gurney equation (eq S6) was used to quantify the charge carrier mobility of the cocrystals that predicts J should scale as applied bias squared (V^2) , assuming the charge transport is governed by the space charge limiting current (SCLC) model. ^{39–42} The representative J versus V^2 plot shows linear dependence (Figure 5e), where the charge carrier mobility (μ) can be calculated from the fitting slope by knowing the crystal height and dielectric constant of the crystal (see section S6, Supporting Information). The calculated charge carrier mobilities of the cocrystals BEADTTF and **BEADPYR** were determined to be $(25.6 \pm 3.1) \times 10^{-5}$ cm² $V^{-1} S^{-1}$ and $(3.5 \pm 0.7) \times 10^{-5} cm^2 V^{-1} S^{-1}$ (Figure 5e). The charge carrier mobility of BEADTTF is thus approximately seven times higher than that for BEA⊃PYR. We attribute more efficient charge mobilities relative to the adduct BEA to the presence of the face-to-face and face-to-edge π -stacks and relatively small band gap energies of the cocrystals. The relative order of the mobilities is consistent with previous mobility data recorded for pure TTF and PYR. 20,21 The mobilities of the cocrystals are also comparable to recently reported cocrystals based on pseudorotaxanes. 14 To the best of our knowledge,

BEADTTF and BEADPYR represent the first examples of boron-based cocrystals that display semiconducting behavior.

In conclusion, we report a strategy to generate semiconductor cocrystals of variable charge carrier mobility. The cocrystals consist of an otherwise nonconductive boronic esterbased B \leftarrow N adduct with aromatic molecules as guests. Our findings support the premise that the incorporation of $\pi\text{-rich}$ molecules into cocrystals with B \leftarrow N adducts carrying electron-deficient ligands generates efficient charge carrier mobility. The cocrystal approach allows establishing persistent face-to-face and face-to-edge $\pi\text{-stacking}$. We envisage the future design of boron-based semiconductor cocrystals with included $\pi\text{-rich}$ guests in related noncovalent framework materials. $^{43-45}$

ASSOCIATED CONTENT

Supporting Information

The Supporting Information is available free of charge at https://pubs.acs.org/doi/10.1021/acs.cgd.9b00953.

Experimental details, conducting probe AFM data, powder and single crystal XRD data (PDF)

Accession Codes

CCDC 1912355–1912356 (for compounds BEA¬TTF and BEA¬PYR) contain the supplementary crystallographic data for this paper. These data can be obtained free of charge via www.ccdc.cam.ac.uk/data_request/cif, or by emailing data_request@ccdc.cam.ac.uk, or by contacting The Cambridge Crystallographic Data Centre, 12 Union Road, Cambridge CB2 1EZ, UK; fax: +44 1223 336033.

AUTHOR INFORMATION

Corresponding Authors

*(A.V.T.) E-mail: alexei-tivanski@uiowa.edu.

*(L.R.M.) E-mail: len-macgillivray@uiowa.edu.

*(H.H.) E-mail: hhopfl@uaem.mx.

ORCID ®

Gonzalo Campillo-Alvarado: 0000-0002-1868-8523

Hugo Morales-Rojas: 0000-0002-9194-6904

Herbert Höpfl: 0000-0002-4027-0131

Leonard R. MacGillivray: 0000-0003-0875-677X

Alexei V. Tivanski: 0000-0002-1528-2421

Author Contributions

*K.K.R. and G.C.-A. contributed equally to this work.

Notes

The authors declare no competing financial interest.

ACKNOWLEDGMENTS

We gratefully acknowledge financial support from the National Science Foundation (L.R.M., DMR-1708673), University of Iowa College of Liberal Arts and Sciences (G.C.-A.), and CONACYT (Project No. 229929 and fellowship for G.C.-A.). The authors acknowledge access to Laboratorio Nacional de Estructura de Macromoléculas (LANEM).

REFERENCES

- (1) Sirringhaus, H. Organic semiconductors: An equal-opportunity conductor. *Nat. Mater.* **2003**, *2*, 641–642.
- (2) Klues, M.; Witte, G. Crystalline packing in pentacene-like organic semiconductors. *CrystEngComm* **2018**, *20*, 63–74.
- (3) Bashir, A.; Heck, A.; Narita, A.; Feng, X.; Nefedov, A.; Rohwerder, M.; Müllen, K.; Elstner, M.; Wöll, C. Charge carrier

mobilities in organic semiconductors: crystal engineering and the importance of molecular contacts. *Phys. Chem. Chem. Phys.* **2015**, *17*, 21988–21996.

- (4) Yao, Z.-F.; Wang, J.-Y.; Pei, J. Control of $\pi-\pi$ stacking via crystal engineering in organic conjugated small molecule crystals. *Cryst. Growth Des.* **2018**, *18*, 7–15.
- (5) Banerjee, A.; Saha, A.; Saha, B. K. Understanding the Behavior of $\pi-\pi$ Interactions in Crystal Structures in Light of Geometry Corrected Statistical Analysis: Similarities and Differences with the Theoretical Models. *Cryst. Growth Des.* **2019**, *19*, 2245–2252.
- (6) Anthony, J. E. Functionalized acenes and heteroacenes for organic electronics. *Chem. Rev.* **2006**, *106*, 5028–5048.
- (7) Anthony, J. E. The larger acenes: versatile organic semi-conductors. *Angew. Chem., Int. Ed.* **2008**, 47, 452–483.
- (8) Wu, Y.; Frasconi, M.; Gardner, D. M.; McGonigal, P. R.; Schneebeli, S. T.; Wasielewski, M. R.; Stoddart, J. F. Electron Delocalization in a Rigid Cofacial Naphthalene-1, 8:4, 5-bis (dicarboximide) Dimer. *Angew. Chem., Int. Ed.* **2014**, 53, 9476–9481.
- (9) Carini, M.; Ruiz, M. P.; Usabiaga, I.; Fernandez, J. A.; Cocinero, E. J.; Melle-Franco, M.; Diez-Perez, I.; Mateo-Alonso, A. High conductance values in π -folded molecular junctions. *Nat. Commun.* **2017**, *8*, 15195.
- (10) Chi, X.; Li, D.; Zhang, H.; Chen, Y.; Garcia, V.; Garcia, C.; Siegrist, T. 5, 6, 11, 12-Tetrachlorotetracene, a tetracene derivative with π -stacking structure: The synthesis, crystal structure and transistor properties. *Org. Electron.* **2008**, *9*, 234–240.
- (11) Miao, Q.; Lefenfeld, M.; Nguyen, T. Q.; Siegrist, T.; Kloc, C.; Nuckolls, C. Self-assembly and electronics of dipolar linear acenes. *Adv. Mater.* **2005**, *17*, 407–412.
- (12) Sokolov, A. N.; Friščić, T.; MacGillivray, L. R. Enforced face-to-face stacking of organic semiconductor building blocks within hydrogen-bonded molecular cocrystals. *J. Am. Chem. Soc.* **2006**, *128*, 2806–2807.
- (13) Mandal, A.; Swain, P.; Nath, B.; Sau, S.; Mal, P. Unipolar to ambipolar semiconductivity switching in charge transfer cocrystals of 2, 7-di-tert-butylpyrene. *CrystEngComm* **2019**, *21*, 981–989.
- (14) Gozalvez, C.; Zafra, J. L.; Saeki, A.; Melle-Franco, M.; Casado, J.; Mateo-Alonso, A. Charge Transport Modulation in Pseudorotaxane 1D Stacks of Acene and Azaacene Derivatives. *Chem. Sci.* **2019**, 10, 2743–2749.
- (15) Herrera-España, A. D.; Campillo-Alvarado, G.; Román-Bravo, P.; Herrera-Ruiz, D.; Höpfl, H.; Morales-Rojas, H. Selective Isolation of Polycyclic Aromatic Hydrocarbons by Self-Assembly of a Tunable N→ B Clathrate. *Cryst. Growth Des.* **2015**, *15*, 1572−1576.
- (16) Cruz-Huerta, J.; Campillo-Alvarado, G.; Höpfl, H.; Rodríguez-Cuamatzi, P.; Reyes-Márquez, V.; Guerrero-Álvarez, J.; Salazar-Mendoza, D.; Farfán-García, N. Self-Assembly of Triphenylboroxine and the Phenylboronic Ester of Pentaerythritol with Piperazine, trans-1,4-Diaminocyclohexane, and 4-Aminopyridine. *Eur. J. Inorg. Chem.* **2016**, 2016, 355–365.
- (17) Campillo-Alvarado, G.; Vargas-Olvera, E. C.; Höpfl, H.; Herrera-España, A. D.; Sánchez-Guadarrama, O.; Morales-Rojas, H.; MacGillivray, L. R.; Rodríguez-Molina, B.; Farfán, N. Self-Assembly of Fluorinated Boronic Esters and 4,4′-Bipyridine into 2:1 N→B Adducts and Inclusion of Aromatic Guest Molecules in the Solid State: Application for the Separation of o, m, p-Xylene. *Cryst. Growth Des.* **2018**, *18*, 2726−2743.
- (18) Min, Y.; Dou, C.; Tian, H.; Geng, Y.; Liu, J.; Wang, L. n-Type Azaacenes Containing $B \leftarrow N$ Units. *Angew. Chem., Int. Ed.* **2018**, *57*, 2000–2004.
- (19) Zhao, R.; Dou, C.; Xie, Z.; Liu, J.; Wang, L. Polymer Acceptor Based on B← N Units with Enhanced Electron Mobility for Efficient All-Polymer Solar Cells. *Angew. Chem., Int. Ed.* **2016**, *55*, 5313−5317.
- (20) Jiang, H.; Yang, X.; Cui, Z.; Liu, Y.; Li, H.; Hu, W.; Kloc, C. Adjusting tetrathiafulvalene (TTF) functionality through molecular design for organic field-effect transistors. *CrystEngComm* **2014**, *16*, 5968–5983.

(21) Suzuki, A.; Inokuchi, H.; Maruyama, Y. Charge-carrier drift mobility in pyrene single crystals. *Bull. Chem. Soc. Jpn.* **1976**, 49, 3347–3348.

- (22) Campillo-Alvarado, G.; D'mello, K. P.; Swenson, D. C.; Santhana Mariappan, S. V.; Hopfl, H.; Morales-Rojas, H.; MacGillivray, L. R. Exploiting Boron Coordination: $B \leftarrow N$ Bond Supports a [2+2] Photodimerization in the Solid State and Generation of a Diboron Bis-Tweezer for Benzene/Thiophene Separation. *Angew. Chem., Int. Ed.* **2019**, 58, 5413–5416.
- (23) Christinat, N.; Croisier, E.; Scopelliti, R.; Cascella, M.; Röthlisberger, U.; Severin, K. Formation of Boronate Ester Polymers with Efficient Intrastrand Charge-Transfer Transitions by Three-Component Reactions. *Eur. J. Inorg. Chem.* **2007**, 2007 (33), 5177–5181.
- (24) Schröder, H. V.; Schalley, C. A. Tetrathiafulvalene—a redox-switchable building block to control motion in mechanically interlocked molecules. *Beilstein J. Org. Chem.* **2018**, *14*, 2163—2185.
- (25) Sun, X.; Brückner, C.; Nieh, M.-P.; Lei, Y. A fluorescent polymer film with self-assembled three-dimensionally ordered nanopores: preparation, characterization and its application for explosives detection. *J. Mater. Chem. A* **2014**, *2*, 14613–14621.
- (26) Nowak, M.; Kauch, B.; Szperlich, P. Determination of energy band gap of nanocrystalline SbSI using diffuse reflectance spectroscopy. *Rev. Sci. Instrum.* **2009**, *80* (4), 046107/1-046107/3.
- (27) Lee, J.-W.; Son, D.-Y.; Ahn, T. K.; Shin, H.-W.; Kim, I. Y.; Hwang, S.-J.; Ko, M. J.; Sul, S.; Han, H.; Park, N.-G. Quantum-dot-sensitized solar cell with unprecedentedly high photocurrent. *Sci. Rep.* **2013**, *3*, 1050.
- (28) Praus, P.; Kozák, O.; Kočí, K.; Panáček, A.; Dvorský, R. CdS nanoparticles deposited on montmorillonite: preparation, characterization and application for photoreduction of carbon dioxide. *J. Colloid Interface Sci.* **2011**, *360* (2), 574–579.
- (29) Ardalan, P.; Brennan, T. P.; Lee, H.-B.-R.; Bakke, J. R.; Ding, I.-K.; McGehee, M. D.; Bent, S. F. Effects of self-assembled monolayers on solid-state CdS quantum dot sensitized solar cells. *ACS Nano* **2011**, *5* (2), 1495–1504.
- (30) Hutchins, K. M.; Rupasinghe, T. P.; Oburn, S. M.; Ray, K. K.; Tivanski, A. V.; MacGillivray, L. R. Remarkable decrease in stiffness of aspirin crystals upon reducing crystal size to nanoscale dimensions via sonochemistry. *CrystEngComm* **2019**, *21*, 2049–2052.
- (31) Kapadia, P. P.; Ditzler, L. R.; Baltrusaitis, J.; Swenson, D. C.; Tivanski, A. V.; Pigge, F. C. Semiconducting organic assemblies prepared from tetraphenylethylene tetracarboxylic acid and bis (pyridine) s via charge-assisted hydrogen bonding. *J. Am. Chem. Soc.* 2011, 133, 8490–8493.
- (32) Reid, O. G.; Munechika, K.; Ginger, D. S. Space Charge Limited Current Measurements on Conjugated Polymer Films using Conductive Atomic Force Microscopy. *Nano Lett.* **2008**, *8*, 1602–1609
- (33) Lee, H. D.; Ray, K. K.; Tivanski, A. V. Solid, Semisolid, and Liquid Phase States of Individual Submicrometer Particles Directly Probed Using Atomic Force Microscopy. *Anal. Chem.* **2017**, *89*, 12720–12726.
- (34) Ray, K. K.; Lee, H. D.; Gutierrez, M. A.; Chang, F. J.; Tivanski, A. V. Correlating 3D Morphology, Phase State, and Viscoelastic Properties of Individual Substrate-Deposited Particles. *Anal. Chem.* **2019**, *91*, 7621–7630.
- (35) Pingree, L. S. C.; Hersam, M. C.; Kern, M. M.; Scott, B. J.; Marks, T. J. Spatially-resolved electroluminescence of operating organic light-emitting diodes using conductive atomic force microscopy. *Appl. Phys. Lett.* **2004**, *85* (2), 344–346.
- (36) Lin, H.-N.; Lin, H.-L.; Wang, S.-S.; Yu, L.-S.; Perng, G.-Y.; Chen, S.-A.; Chen, S.-H. Nanoscale charge transport in an electroluminescent polymer investigated by conducting atomic force microscopy. *Appl. Phys. Lett.* **2002**, *81* (14), 2572–2574.
- (37) Liau, Y.-H.; Scherer, N. F.; Rhodes, K. Nanoscale Electrical Conductivity and Surface Spectroscopic Studies of Indium-Tin Oxide. *J. Phys. Chem. B* **2001**, *105* (16), 3282–3288.

(38) Ionescu-Zanetti, C.; Mechler, A.; Carter, S. A.; Lal, R. Semiconductive polymer blends: correlating structure with transport properties at the nanoscale. *Adv. Mater. (Weinheim, Ger.)* **2004**, *16* (5), 385–389.

- (39) Blom, P. W. M.; de Jong, M. J. M.; Vleggaar, J. J. M. Electron and hole transport in poly(p-phenylene vinylene) devices. *Appl. Phys. Lett.* **1996**, *68*, 3308–3310.
- (40) Moreno-Moreno, M.; Ares, P.; Moreno, C.; Zamora, F.; Gomez-Navarro, C.; Gomez-Herrero, J. AFM Manipulation of Gold Nanowires To Build Electrical Circuits. *Nano Lett.* **2019**, *19* (8), 5459–5468.
- (41) Mott, N. F.; Gurney, R. W. Electronic Processes in Ionic Crystals, 2nd ed.; Clarendon Press: Oxford, 1940.
- (42) Murgatroyd, P. Theory of space-charge-limited current enhanced by Frenkel effect. *J. Phys. D: Appl. Phys.* **1970**, 3 (2), 151–156.
- (43) Stephens, A. J.; Scopelliti, R.; Tirani, F. F.; Solari, E.; Severin, K. Crystalline Polymers Based on Dative Boron—Nitrogen Bonds and the Quest for Porosity. *ACS Mater. Lett.* **2019**, *1*, 3–7.
- (44) Fornasari, L.; Mazzaro, R.; Boanini, E.; D'Agostino, S.; Bergamini, G.; Grepioni, F.; Braga, D. Self-Assembly and Exfoliation of a Molecular Solid Based on Cooperative B–N and Hydrogen Bonds. *Cryst. Growth Des.* **2018**, *18*, 7259–7263.
- (45) Campillo-Alvarado, G.; D'mello, M. M.; Sinnwell, M. A.; Höpfl, H.; Morales-Rojas, H.; MacGillivray, L. R. Channel Confinement of Aromatic Petrochemicals via Aryl—Perfluoroaryl Interactions With a $B \leftarrow N$ Host. Front. Chem. **2019**, 7, 695.